Chemosphere 234 (2019) 690–701

Contents lists available at ScienceDirect

Chemosphere

journal homepage: www.elsevier.com/locate/chemosphere

Sorption of phosphate and silicate alters dissolution kinetics of poorly crystalline iron (oxyhydr)oxide

Peter Kraal [a, b, *], Case M. van Genuchten [a], Thilo Behrends [a], Andrew L. Rose [c]

[a] Department of Earth Sciences – Geochemistry, Faculty of Geosciences, Utrecht University, PO Box 80021, 3508, TA, Utrecht, the Netherlands
[b] Royal Netherlands Institute for Sea Research, Department of Ocean Systems, and Utrecht University, P.O. Box 59, 1790, AB, Den Burg, the Netherlands
[c] School of Environment, Science and Engineering, Southern Cross University, PO Box 157, Lismore NSW, Australia

HIGHLIGHTS

- P and Si coprecipitation subtly altered Fe (oxyhydr)oxide (FeOx) structure.
- Coprecipitation of P and Si markedly enhanced FeOx dissolution rate.
- Adsorption onto pre-existing FeOx did not change structure but slowed dissolution.
- Environmental fate of FeOx and nutrients affected by interaction mechanism.
- Eutrophication can lead to less stabile FeOx and more intense nutrient regeneration.

ARTICLE INFO

Article history:
Received 25 March 2019
Received in revised form
3 June 2019
Accepted 10 June 2019
Available online 21 June 2019

Handling Editor: Martine Leermakers

ABSTRACT

Iron (oxyhydr)oxides (FeOx) control retention of dissolved nutrients and contaminants in aquatic systems. However, FeOx structure and reactivity is dependent on adsorption and incorporation of such dissolved species, particularly oxyanions such as phosphate and silicate. These interactions affect the fate of nutrients and metal(loids), especially in perturbed aquatic environments such as eutrophic coastal systems and environments impacted by acid mine drainage. Altered FeOx reactivity impacts sedimentary nutrient retention capacity and, eventually, ecosystem trophic state. Here, we explore the influence of phosphate (P) and silicate (Si) on FeOx structure and reactivity. Synthetic, poorly crystalline FeOx with adsorbed and coprecipitated phosphate or silicate at low but environmentally relevant P/Fe or Si/Fe ratios (0.02–0.1 mol mol^{-1}) was prepared by base titration of Fe(III) solutions. Structural characteristics of FeOx were investigated by X-ray diffraction, synchrotron-based X-ray absorption spectroscopy and high-energy X-ray scattering. Reactivity of FeOx was assessed by kinetic dissolution experiments under acidic (dilute HCl, pH 2) and circum-neutral reducing (bicarbonate-buffered ascorbic acid, pH 7.8, $E_h \sim -300$ mV) conditions. At these loadings, phosphate and silicate coprecipitation had only slight impact on local and intermediate-ranged FeOx structure, but significantly enhanced the dissolution rate of FeOx. Conversely, phosphate and silicate adsorption at similar loadings resulted in particle surface passivation and decreased FeOx dissolution rates. These findings indicate that varying nutrient loadings and different interaction mechanisms between anions and FeOx (adsorption versus coprecipitation) can influence the broader biogeochemical functioning of aquatic ecosystems by impacting the structure and reactivity of FeOx.

1. Introduction

Iron minerals such as ferric iron (oxyhydr)oxides (here, referred to as FeOx), play a crucial role in the biogeochemical cycling and mobility of nutrients, trace elements and contaminants in aquatic systems. Ferrihydrite (Fh), $Fe_{10}O_{14}(OH)_2 \cdot nH_2O$ with $n < 1$ according to the most recent model (Michel et al., 2007; Hiemstra, 2013), is a

* Corresponding author. Royal Netherlands Institute for Sea Research, Department of Ocean Systems, and Utrecht University, P.O. Box 59, 1790, AB, Den Burg, the Netherlands.
E-mail address: peter.kraal@nioz.nl (P. Kraal).

https://doi.org/10.1016/j.chemosphere.2019.06.071
0045-6535/

particularly reactive FeOx that forms in soils and sediments by rapid Fe^{2+} oxidation or Fe^{3+} hydrolysis (Jambor and Dutrizac, 1998). Although Fh is thermodynamically unstable, its crystallization to more stable phases such as lepidocrocite and goethite can be inhibited in the presence of anions and organic compounds (Schwertmann and Cornell, 1991; Jones et al., 2009; Voegelin et al., 2013; Senn et al., 2017). Ferrihydrite has a high affinity for sorption of oxyanions of arsenic (As), phosphorus (P) and silicate (Si), which are environmentally significant as nutrients and/or contaminants. Consequently, Fh plays an important role in (i) scavenging and retention of nutrients in freshwater and marine systems (Buffle et al., 1989; Norkko et al., 2012), and (ii) retardation of toxic metal(loid) transport in surface waters that are contaminated by mining activities (Rose and Ghazi, 1998; Webster et al., 1998).

Interaction with oxyanions in solution can alter the structure and reactivity of Fh (Waychunas et al., 1993; Paige et al., 1997b; Majzlan, 2011) either through adsorption (binding of oxyanions onto pre-existing Fh surfaces) and coprecipitation (FeOx nucleation and particle growth in the presence of oxyanions). Adsorption of oxyanions has a relatively minor effect on FeOx mineral structure (Waychunas et al., 1993; van Genuchten and Peña, 2016), but decreases mineral reactivity and solubility by forming multi-nuclear inner-sphere complexes with surface groups (Biber et al., 1994; Stumm, 1997). This can thermodynamically stabilize the Fh surface (Majzlan, 2011) and retard the crystallization of Fh to goethite and hematite (Cornell et al., 1987; Paige et al., 1997b). Furthermore, adsorption of phosphate onto Fh at concentrations sufficient to saturate surface sites has been shown to lead to a three-fold decrease in the Fh reduction rate by the bacterium *Shewanella putrefaciens* (CN32) in microbial incubation experiments (Borch et al., 2007). In a recent study, a marked decrease in the rate and extent of microbially-mediated reductive dissolution of schwertmannite, a poorly ordered Fe(III) oxyhydroxysulfate, with increasing P surface coverage was observed (Schoepfer et al., 2017). The stabilization of the FeOx surface by oxyanion sorption and subsequent decrease in the rate of reductive Fe dissolution may modulate benthic Fe release and thus affect Fe availability in aquatic systems.

Coprecipitation differs from adsorption in that oxyanions interact with Fe polyhedra during nucleation and thereby alter the final mineral structure. Increased disorder of FeOx formed in the presence of oxyanions such as AsO_4, phosphate and silicate has been observed during rapid Fe(III) hydrolysis in highly concentrated (~0.5 mol L^{-1}) Fe(III) solutions (Waychunas et al., 1993; Rose et al., 1996) as well as during oxygenation of less concentrated (<1 m mol L^{-1}) Fe(II) solutions (Voegelin et al., 2010; van Genuchten et al., 2014; Senn et al., 2015, 2017). Occupation of FeOx surface sites by P or Si disrupts Fe–Fe polymerization and leads to the formation of relatively small, poorly ordered FeOx polymers with relatively large surface areas. Decreased order, greater surface area and difference in particle charge suggest that oxyanion coprecipitation would enhance the reactivity and solubility of Fh. Indeed, Kukkadapu et al. (2004) found that incorporation of even small amounts of Si in Fh (Si/(Si + Fe) = 0.01–0.05 mol mol^{-1}) increased the extent of Fh reduction by *Shewanella putrefaciens* over 1 week about 5-fold. Conversely, coprecipitation of oxyanions such as arsenate (AsO_4), phosphate and silicate has been shown to strongly inhibit the crystallization of Fh (Cornell et al., 1987; Paige et al., 1997b; Senn et al., 2017). Furthermore, Paige et al. (1997a) reported that As coprecipitation decreased the rate of Fh dissolution under acidic conditions. As such, the stabilizing effect of adsorption of oxyanions onto the FeOx surface seems well-established, but the impact of oxyanion coprecipitation on FeOx reactivity is not well understood.

Here, we investigate the impact of the adsorption and coprecipitation of phosphate and silicate on the structure and dissolution kinetics of FeOx, formed by base titration of Fe(III) solutions, under acidic (pH 2) and circum-neutral (pH 7.8) reducing conditions. Our results show a subtle impact of oxyanion coprecipitation on FeOx structure, but marked and opposite effects of adsorption and coprecipitation on the rate of FeOx dissolution.

2. Materials and methods

2.1. Synthesis of 2L-Fh

Pure two-line ferrihydrite (2L-Fh, denoted here as pure FeOx) was synthesized following the procedure of Schwertmann and Cornell (1991) with NaOH as base. In short, 40 g of Fe(III)(NO_3)$_3$·$9H_2O$ (Merck EMSURE) was dissolved in 500 mL degassed ultrapure H_2O (initial Fe concentration ~0.2 mol L^{-1}) in a HDPE beaker and the pH was subsequently brought to a stable value of 7.5 with 1 mol L^{-1} NaOH that was titrated at a maximum rate of 20 mL min^{-1} using a Metrohm Titrando 809 equipped with a plastic (ETFE) Dosino 800 burette. The pH was considered stable when ΔpH <0.01 over a 10-min period. The total volume of added 1 mol L^{-1} NaOH was ~330 mL. The suspension was bubbled with Ar throughout the synthesis procedure to avoid the introduction of CO_2. The precipitate was transferred into Spectra/Por 4 regenerated cellulose dialysis tubing (SpectrumLabs) and dialyzed in 10 L of ultrapure water with regular water changes until the electric conductivity was <10 μS cm^{-1} (4 days).

2.2. Silicate and phosphate sorption curves

Sorption of P and Si onto 2L-Fh was examined at pH 6, 7 and 8 using a 13-point concentration gradient over the range 0–2500 μmol P or Si L^{-1} at each pH. The data were fit using the Freundlich and Langmuir equations. More information on chemical and experimental conditions for the sorption curves can be found in the supplementary information.

2.3. Synthesis of 2L-Fh with adsorbed phosphate or silicate

Two-line ferrihydrite with phosphate or silicate adsorbed to the mineral surface (denoted as P-ads FeOx and Si-ads FeOx, respectively) was prepared by addition of P or Si to the dialyzed 2L-Fh suspension as follows. Four separate experiments were conducted to obtain 2L-Fh with "high" and "low" P or Si surface loading (Table 1), roughly corresponding to ~ 25% and 65% surface coverage assuming the asymptotic maxima of the P and Si sorption curves (Fig. S1) represent saturation of surface sites. Due to the lower adsorption maximum of Fh for Si compared to P, the Si/Fe ratios corresponding to low and high Si loading are lower than the P/Fe ratios. In LDPE bottles, 15 mL of the pure 2L-Fh suspension was added to 500 mL of degassed 0.7 mol L^{-1} NaCl with an appropriate concentration of sodium phosphate ($Na_2HPO_4·7H_2O$) or sodium metasilicate ($Na_2SiO_3·9H_2O$). The pH was measured with a calibrated Orion glass pH electrode and adjusted to 7 with small additions of concentrated HCl or NaOH. The suspensions were shaken horizontally at 100 rpm for 92 h (pH readjusted after 48 h), after which the suspensions were allowed to settle for 2 h and the clear supernatant was decanted. The remaining suspension was transferred into 50 mL polypropylene tubes, which were centrifuged at 2500 rpm for 5 min, after which the supernatant was decanted. The resulting slurries were washed three times by resuspension in 250 mL 0.7 mol L^{-1} NaCl followed by centrifugation and decantation, and afterwards resuspended in 15 mL 0.7 mol L^{-1} NaCl to obtain the original suspension density.

FeOx with coprecipitated P or Si was synthesized by rapid

hydrolysis of Fe(III) in the presence of P or Si. For consistency in the manuscript, we refer to these species as P-cop FeOx and Si-cop FeOx. These FeOx were prepared with target molar P/Fe or Si/Fe ratios of 1/10 and 1/20, respectively (Table 1). For this, appropriate amounts of $Na_2HPO_4 \cdot 7H_2O$ or $Na_2SiO_3 \cdot 9H_2O$ were added to the degassed 1 mol L^{-1} NaOH solutions prior to Fe(III) hydrolysis by base titration. The various precipitates were dialyzed in separate water baths and stored in suspension in the dark at 4 °C. The dissolution experiments (section 2.4) started immediately after synthesis of all required minerals. The final concentration in all suspensions was 25–30 mg FeOx mL^{-1}. An overview of all FeOx samples used in this study is given in Table 1.

2.4. Characterization of FeOx

From all FeOx suspensions, a subsample was freeze-dried and ground immediately after dialysis. For regular 2L-Fh, another subsample was freeze-dried after ~4 weeks of storage ("aged" 2L-Fh) to check for aging effects. In addition, a ~10 mg subsample of each FeOx was dissolved in 1 mL concentrated suprapur HCl overnight with subsequent 10-fold dilution with ultrapure H_2O for measurements of Fe, P and Si. The Fe contents of the acid digests were determined colorimetrically by the 1,10-phenanthroline (Fe) (APHA, 2005), P or Si content were quantified using the molybdenum blue method (Mullin and Riley, 1955; Strickland and Parsons, 1972). Absorbance was measured with a Shimadzu UV-1800 spectrophotometer.

Subsamples of the freeze-dried and ground FeOx were analyzed with a Bruker-AXS D2 Phaser powder X-ray diffractometer equipped with Lynxeye detector and Cobalt $K\alpha_{1,2}$ radiation source. For Fe K-edge extended X-ray absorption fine structure (EXAFS) spectroscopy measurements, a second series of subsamples of the freeze-dried and ground FeOx was thoroughly mixed with small quantities of microcrystalline cellulose (Sigma Aldrich) by manual grinding with an agate mortar and pestle. Part of the mixture, containing the amount of sample for which Fe absorption was about 1 absorption length (Kelly et al., 2008), was pressed into 7 mm-diameter pellets (thickness ~1 mm) using a hand-held hydraulic pellet press (Pike Technologies). The pellets were transported to the European Synchrotron Radiation Facility (ESRF) in Grenoble (France) to collect Fe K-edge EXAFS spectra at beamline BM26A (DUBBLE). Details on the beamline setup can be found in Borsboom et al. (1998) and Nikitenko et al. (2008). At the beamline, the pellets were sealed between two layers of Kapton tape and mounted onto the sample holder. Spectra were recorded at room temperature in transmission mode from 6962 to 7862 eV, corresponding to a maximum k of 13 $Å^{-1}$ in the EXAFS region. The vertical dimension of the X-ray beam was 1 mm, the horizontal dimension was 3 mm and the X-ray beam was detuned 30% to prevent second-order harmonics. The near-edge X-ray absorption (XANES) region was measured with 0.35 eV steps, whereas step sizes of 0.05 $Å^{-1}$ were used for the EXAFS region. Two scans were collected for each sample. A Fe(0) foil was used to calibrate the energy of the beam by adjusting the maximum slope of the Fe main edge to 7112 eV. Spectra were averaged, and background-subtracted using the software package Athena (Ravel and Newville, 2005). The EXAFS spectra were extracted using k^3-weighting and were Fourier-transformed over the k-range 2–11 $Å^{-1}$ using a Kaiser-Bessel window with dk of 3 $Å^{-1}$. Spectra were compared to those of Fe reference materials collected during previous synchrotron visits (Kraal et al., 2017).

For the collection of high-energy X-ray scattering (HEXS) data suitable for pair distribution function (PDF) analysis, a third series of subsamples were ground using an agate mortar and pestle and loaded into Kapton capillaries. HEXS data were collected at room temperature at beamline 11-ID-B of the Advanced Photon Source (APS) at Argonne National Laboratory (Argonne, Illinois, USA). The X-ray energy during data collection was 58.9 keV and data were collected out to a Q value near 29 $Å^{-1}$. Scattering patterns were corrected for sample-to-detector distance, tilt angle of the detector with respect to the direction of the incident beam, and X-ray polarization and integrated radially using the Fit2D program (Hammersley et al., 1996). The PDFGetX2 program (Farrow et al., 2007) was used to extract the total structure function (S(Q)) and the PDF (G(r)) using standard procedures (Chupas et al., 2003).

Table 1
Description and composition of ferric iron (oxyhydr)oxides (FeOx) synthesized for this study. For the (P, Si)/Fe ratios, the standard deviation of triplicate analyses is given between parentheses.

Name	Description	Measured (P, Si)/Fe ($mol\ mol^{-1}$)
pure FeOx	2-line ferrihydrite (Fh)	–
P5-cop FeOx	FeOx with low coprecipitated P	0.05 (0.00)
P9-cop FeOx	FeOx with high coprecipitated P	0.09 (0.00)
P5-ads FeOx	2-line Fh with low adsorbed P	0.05 (0.00)
P10-ads FeOx	2-line Fh with high adsorbed P	0.10 (0.00)
Si4-cop FeOx	FeOx with low coprecipitated Si	0.04 (0.00)
Si9-cop FeOx	FeOx with high coprecipitated Si	0.09 (0.00)
Si2-ads FeOx	2-line Fh with low adsorbed Si	0.02 (0.00)
Si7-ads FeOx	2-line Fh with high adsorbed Si	0.07 (0.00)

2.5. Acidic and reductive dissolution experiments

The dissolution kinetics of the various synthesized FeOx was studied under acidic (pH 2) conditions (acidic dissolution experiment; ADE) and circum-neutral (pH 7.8) reducing conditions (reductive dissolution experiment; RDE). The dissolution experiments were performed using polyethylene terephthalate (PET) bottles and included duplicates for each FeOx. The samples were divided over four experimental runs in the order: ADE P-bearing FeOx, ADE Si-bearing FeOx, RDE P-bearing FeOx, RDE Si-bearing FeOx. All four runs included 2L-Fh as reference. Runs were started consecutively with two-week intervals. Total Fe, P and Si concentrations in the ADE and RDE were determined colorimetrically in unfiltered samples from the PET bottles that were taken after thorough homogenization and acidified to pH 0 for 16 h in order to dissolve all FeOx.

For the ADE, 2 mL of FeOx suspension (~50 mg FeOx) was introduced into 500 mL of 0.01 mol L^{-1} suprapur HCl (pH 2). The pH was checked regularly throughout the experiment and did not deviate significantly from the target value of 2. The suspensions were continuously stirred by Teflon-coated floating stir bars on an IKA RO15 magnetic stirrer (400 rpm). After set time intervals, a 2 mL sample was taken from each bottle using a 10 mL syringe and filtered over 0.2 μm Nylon filter membranes. A 500 μL subsample of this filtrate was immediately brought to pH 4 using 500 μL of 3 mol L^{-1} acetic acid/3 mol L^{-1} sodium acetate in polystyrene cuvette, in order to slow down acidic dissolution. Preliminary experiments had shown negligible FeOx dissolution at pH 4 over several days. The light absorbance of this mixture at 430 nm was recorded. Immediately afterwards, 25 μL of a 5 mM stock of the selective Fe(III) chelator desferrioxamine B (DFO-B, Sigma Aldrich) was added and after 10 min the light absorbance was again measured at 430 nm. Preliminary testing has shown that this time period was required for complete reaction between dissolved Fe(III) and DFO-B in solutions of similar chemical composition. Desferrioxamine B binds dissolved and weakly complexed Fe(III) in seconds to minutes, while it binds more strongly complexed Fe on

longer timescales (hours) (Pham et al., 2006). The absorbance measured after 10 min was used as a measure of the pool of dissolved and weakly complexed Fe(III) in the filtrates, denoted here as $Fe(III)_{dissolved}$. After 72 h, the final absorbance value in the DFO-B samples was used as measure for total Fe(III) < 0.2 μm in the filtrates, denoted as $Fe(III)_{<0.2\mu m}$. The difference between $Fe(III)_{<0.2\mu m}$ and $Fe(III)_{dissolved}$ was assumed to represent Fe present in small (<0.2 μm), relatively stable complexes and denoted here as $Fe(III)_{colloid}$. Preliminary tests showed that addition of the pH 4 buffer to samples did not affect this speciation. Immediately after the Fe measurements, P and Si were determined colorimetrically on separate subsamples of the pH-buffered filtrates.

For the RDE, 4 mL of FeOx suspension (~100 mg of FeOx) was added to 500 mL of a solution containing 50 g L^{-1} sodium citrate ($C_6H_5Na_3O_7$), 50 g L^{-1} sodium bicarbonate ($NaHCO_3$) and 20 g L^{-1} ascorbic acid ($C_6H_8O_6$) solution with a final pH of 7.8 and an E_h of ~ −300 mV (prepared using Ar-purged ultrapure H_2O). Ferric iron dissolved in this reducing solution may be a reasonable estimate for Fe(III) available for microbial dissimilatory Fe reduction (Hyacinthe et al., 2006). The suspensions were continuously stirred and purged with Ar to avoid introduction of O_2 over the course of the experiment. At set time intervals, 6 mL samples were taken and filtered over 0.2 μm Nylon filter membranes. Dissolved Fe(II) ($Fe(II)_{dissolved}$) was immediately determined in a subsample of the filtrate with the 1,10-phenanthroline (Sigma Aldrich) colorimetric method. Total Fe < 0.2 μm ($Fe_{<0.2\mu m}$) was measured after addition of an aliquot of 100 g L^{-1} hydroxylamine-HCl (Merck) reducing agent and overnight reaction. The difference between $Fe_{<0.2\mu m}$ and $Fe(II)_{dissolved}$ was assumed to represent small complexes ($Fe_{colloid}$). In addition, soluble reactive P and Si were determined on separate subsamples using the molybdenum blue methods. Relative errors from duplicate experiments were generally <5% for Fe and P, and up to 10% for Si.

2.6. Equations for FeOx dissolution kinetics

In order to facilitate the comparison of dissolution rates between experiments, the rates as function of reaction progress were obtained using the equation described in Postma (1993) and Larsen and Postma (2001):

$$J = km_0 f(m/m_0)g(C) \quad (1)$$

where J represents the overall rate of dissolution (mol s^{-1}), k represents the rate constant (s^{-1}), m_0 represents the initial amount of FeOx (mol) and m represents the amount of undissolved FeOx (mol). In addition, $f(m/m_0)$ is a function of changing FeOx characteristics during dissolution (particle size, morphology, site density), and $g(C)$ is a function of solution composition, accounting for kinetic effects of reactions at the FeOx surface. In concentrated solutions as used in the ADE and RDE, $g(C)$ can be considered constant and equation (1) reduces to:

$$J/m_0 = k'(m/m_0)^{\gamma} \quad (2)$$

where $k' = kg(C)$ and γ represents the fitting parameter describing the changing particle properties during dissolution. Equation (2) can be integrated and rewritten as:

$$m/m_0 = \left[-k'(1-\gamma)t + 1 \right]^{\frac{1}{1-\gamma}} \quad (3)$$

Values of k' and γ were obtained by non-linear least squares regression fitting of the experimentally determined m/m_0 versus t data using the software package R (R.Core.Team, 2013).

3. Results

3.1. Characterization of FeOx

The P/Fe and Si/Fe ratios for the various FeOx are shown in Table 1. The XRD spectra of all FeOx showed two broad peaks, centered around ~40 and 75 °2Θ that are characteristic for 2-line ferrihydrite (data not shown). The peak amplitudes were slightly lower for P9-cop FeOx compared to all other FeOx.

Iron K-edge EXAFS spectra showed subtle differences between 2L-Fh and P-cop/Si-cop FeOx at the highest oxyanion loading (Fig. 1A − C). The shoulder feature at $k = 5.1$ $Å^{-1}$, a characteristic feature of 2L-Fh that is not observed in the Fe K-edge EXAFS spectra of less ordered Fe(III) precipitates (Voegelin et al., 2010; van Genuchten et al., 2014), was slightly weaker in the P9-cop and Si9-cop FeOx samples than for pure FeOx. In addition, the second (R+ΔR = 2.4 Å) and third (R+ΔR = 3.1 Å) peak in the Fourier-transformed spectra (Fig. 1D − F) that represent edge-sharing and corner-sharing Fe octahedra, respectively (Voegelin et al., 2010; van Genuchten et al., 2014), were smaller for P9-cop FeOx and Si9-cop FeOx than for pure FeOx. This suggests decreased structural order or a lower degree of polymerization compared to pure FeOx (Voegelin et al., 2010). There were no significant differences in the Fe K-edge EXAFS spectra for pure FeOx and P-ads/Si-ads FeOx (data not shown).

The pair distribution functions (PDFs) obtained from HEXS showed an overall decrease in peak amplitude for FeOx with coprecipitated P or Si compared to pure FeOx (Fig. 2A). There were only very minor differences between the PDFs of fresh and aged pure FeOx. Subtracting the PDF of pure FeOx (here, the mean of the very similar spectra for fresh and aged 2L-Fh) from the PDFs for the P-cop FeOx and Si-cop FeOx further emphasizes the structural changes by coprecipitation of P and Si during FeOx formation (Fig. 2B). The P-cop and Si-cop FeOx showed relatively high amplitudes (i.e. a positive ΔG) at ~1.6 and ~3.2 Å, indicative of P/Si—O and P/Si—Fe bonds respectively (van Genuchten et al., 2014). Moreover, a relatively low amplitude for P-cop FeOx and Si-cop FeOx was observed at ~3.4 Å, the interatomic distance of corner-sharing Fe—Fe bonds. Peak heights generally decreased in the order: pure FeOx > P4-cop FeOx ≈ Si4-cop FeOx > Si9-cop FeOx > P9-cop FeOx. The maximum interatomic distance at which well-defined peaks are evident in the PDFs, which is a measure for nanoparticle dimensions (Chapman and Chupas, 2013), was ~2 nm for all FeOx except P9-cop FeOx (~1.5 nm).

3.2. Sorption of phosphate and silicate by ferrihydrite

Sorption of phosphate onto pure FeOx reached an asymptotic maximum of ~2000 μmol P per g FeOx at pH 7 (the pH used for synthesis of P-ads and Si-ads Fh for the ADE and RDE). The high maximum concentration of adsorbed Si most likely was the result of Si polymerization at the FeOx surface at the high end of the Si sorption curve (Fig. S1B). Fitting a sorption curve only to data for Si/Fe ratios at which Si polymerization was likely insignificant suggested a sorption capacity of ~1000 μmol Si per g FeOx. Further information on the results of the sorption experiments can be found in the Supplementary Information.

3.3. Acidic and reductive FeOx dissolution

The dissolution of (P- and Si-bearing) FeOx was assessed from the accumulation of Fe, P and Si in solution (consisting of dissolved and colloidal species < 0.2 μm) (Figs. 3 and 4). From the $Fe(III)_{dissolved}$ and $Fe(II)_{dissolved}$ values obtained from ADE and RDE, respectively (see section 2.5), dissolution rates for each type of

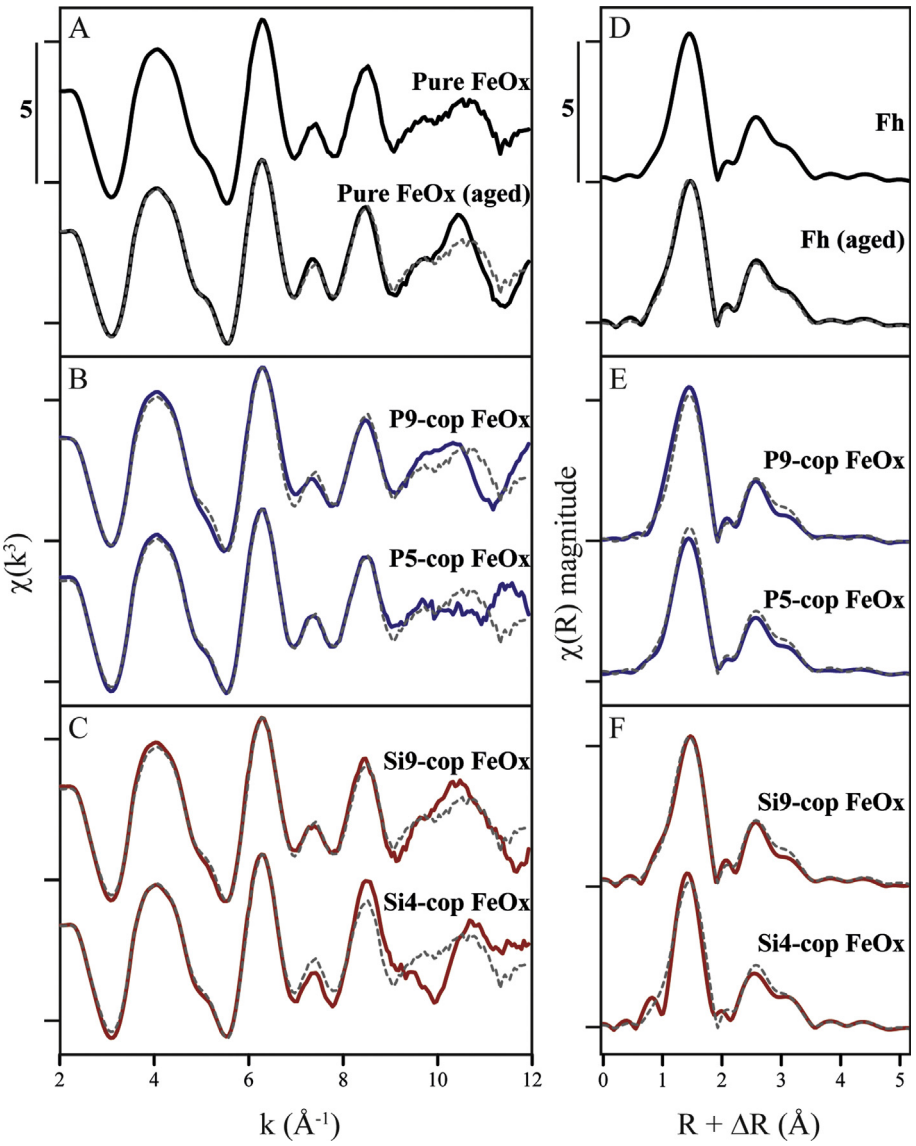

Fig. 1. Iron K-edge EXAFS spectra (A–C) and Fourier-transformed iron K-edge EXAFS spectra (D–F) of the various synthesized hydrous ferric oxides. The plots for FeOx with coprecipitated P or Si show the spectrum of fresh pure FeOx as gray dashed line for reference.

FeOx were calculated as described in section 2.6 and fitting parameters are shown in Table 2. The normalized rates (J/m_0) are presented as a function of the remaining fraction of FeOx, m/m_0 (Fig. 5). For all FeOx, the dissolution rate decreased with progressing FeOx dissolution. While standard deviation of replicate measurements of any FeOx within a run was small (error bars in Figs. 3 and 4), there were relatively large differences in 2L-Fh dissolution behavior between runs (Figs. 3–5; for explanation on the runs see section 2.5). P-cop FeOx and Si-cop FeOx showed enhanced dissolution rates compared to pure FeOx under both acidic and reductive conditions. These FeOx generally showed fastest dissolution rates at the highest oxyanion loading for both ADE and RDE (except for Si-cop FeOx in RDE). Consistent with the dissolution rate, the fraction of FeOx dissolved at the end of ADE and RDE was higher for P-cop and Si-cop FeOx compared to pure FeOx.

Adsorption of P and Si initially caused decreased FeOx dissolution rates under both acidic and reducing conditions (Figs. 3 and 4). At the end of ADE and RDE, however, the fraction of dissolved Fe for P-ads FeOx and Si-ads FeOx was comparable to or higher than that for pure FeOx (70–80%), with the exception of P10-ads FeOx in ADE experiments (50%). That is, the highest loading with adsorbed P retarded acidic FeOx dissolution throughout the whole experiment, which was reflected by a relatively high γ value for P10-ads FeOx in ADE (Table 2). In all other experiments with adsorbed P and Si, the retardation was only effective at the beginning and was compensated towards the end of the experiment.

For pure FeOx during both ADE and RDE, $Fe_{colloid}$ shows a strong increase during the first few hours of the dissolution experiments, up to ~60% of total Fe, and a subsequent decrease to a fraction of 20–40% that is relatively stable for the remainder of each experiment (Fig. 3A, F; Fig. 4A, F). During acidic dissolution of FeOx, coprecipitated and adsorbed P suppresses the release of $Fe_{colloid}$ (Fig. 3B – E). Such inhibition of $Fe_{colloid}$ accumulation is also observed for adsorbed Si – be it to a lesser extent – but not coprecipitated Si under acidic conditions (Fig. 3G – J). During reductive dissolution, temporal trends in the relative contribution of $Fe_{colloid}$ were less apparent, apart from a relatively fast

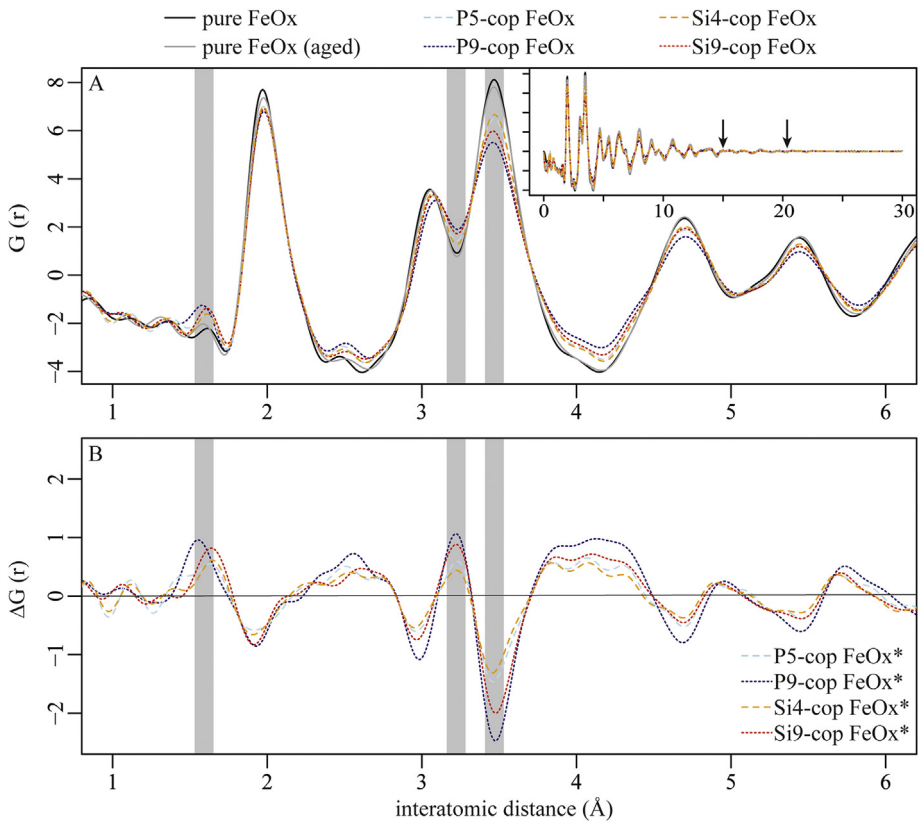

Fig. 2. (A) Atomic pair distribution functions (PDF) of synthesized FeOx determined by high energy X-ray scattering, HEXS. The results are plotted out to 6 Å, focusing on local structure (i.e. the first few coordination spheres). The inset in panel A shows the full-range PDFs, where arrows indicate the maximum interatomic distance at which well-defined peaks are evident in the PDF for P9-cop FeOx (~1.5 nm) and all other FeOx (~2 nm). (B) PDFs for FeOx with coprecipitated P or Si plotted as difference between the FeOx spectrum and that of the mean of the two 2L-Fh spectra. Vertical gray bars indicate key atomic distances where the amplitude in the PDF is different for the P- and Si-cop FeOx compared to pure FeOx: ~1.6 Å (Si/P–O), ~3.2 Å (Si/P–Fe) and 3.4 Å (Fe–Fe).

accumulation for P-cop FeOx compared to all other FeOx.

Under acidic conditions, release of P and Si from the solid phase into solution lagged release of $Fe(III)_{dissolved}$ (Fig. 3D–E, I-J). The lag time was greater for P-ads FeOx than P-cop FeOx. For adsorbed P, the lag was most pronounced at higher P loading. The incongruent dissolution resulted in high initial Fe/P ratios in solution during the first hours (up to 10 h, for P5-ads FeOx) that later declined to values more representative of the bulk FeOx composition. The Si-bearing FeOx showed no such lag effect during acidic dissolution; the release of Si into solution exceeded that of (total) Fe, particularly during the early stages of FeOx dissolution. As a result, the Fe/Si ratio in solution was initially low and gradually increased over the course of Si-cop FeOx dissolution. No such lag effect was observed for RDE, during which P and Si accumulation in solution was rapid and initially exceeded the rate of Fe accumulation (Fig. 4).

4. Discussion

4.1. The impact of oxyanion coprecipitation on FeOx structure

Two main pathways of FeOx precipitation are Fe(II) oxidation and Fe(III) hydrolysis. Previous work has shown that the presence of even small amounts of oxyanions such as phosphate and silicate can alter the structure of FeOx formed during Fe(II) oxidation. This arises from the occupation of binding sites by the oxyanions during FeOx nucleation, which hinders FeO_6 polymerization and FeOx crystallization (Voegelin et al., 2010; van Genuchten et al., 2014; Senn et al., 2015). In particular, the Fe(II)-catalyzed crystallization of poorly ordered FeOx is inhibited (Boland et al., 2014) and as a result, poorly ordered FeOx persists in the presence of P and Si over experimental durations of 2–5 h during Fe(II) oxidation. This effect of P and Si coprecipitation has been observed at initial P/Fe ratios down to 0.02 (Voegelin et al., 2010). Sorption of oxyanions such as phosphate and silicate onto FeOx surface sites can effectively stabilize poorly ordered FeOx and inhibit their transformation to more crystalline phases over long timescales of at least days to weeks (Cornell et al., 1987; Paige et al., 1997b; Senn et al., 2017). As such, the transformation kinetics of FeOx depend critically on the chemical conditions under which they exist.

In contrast to Fe(II) oxidation experiments, the presence of oxyanions is shown to have more subtle effect on the structure of FeOx formed by Fe(III) hydrolysis from concentrated solution (Fe(III) > 100 mM). This is partly because Fe(II)-catalyzed crystallization processes do not play a role under the latter experimental conditions. When FeOx forms by the hydrolysis of Fe(III) solutions, coprecipitated oxyanions affect FeOx formation by occupation of crystal growth sites during Fe(III) polymerization. This “poisoning” of FeOx surface sites interferes with Fe–Fe bond formation and decreases the structural coherency of already poorly ordered FeOx (2L-Fh) formed by Fe(III) hydrolysis at circumneutral pH. This effect is reflected in Fourier-transformed Fe EXAFS data of FeOx with coprecipitated P or Si by decreased magnitude peaks for Fe–Fe interatomic pairs, most notably corner-sharing bonds, and a strong disruption of Fe–Fe bond formation at oxyanion/Fe ratios >0.2 (Waychunas et al., 1993; Rose et al., 1996; Pokrovski et al., 2003).

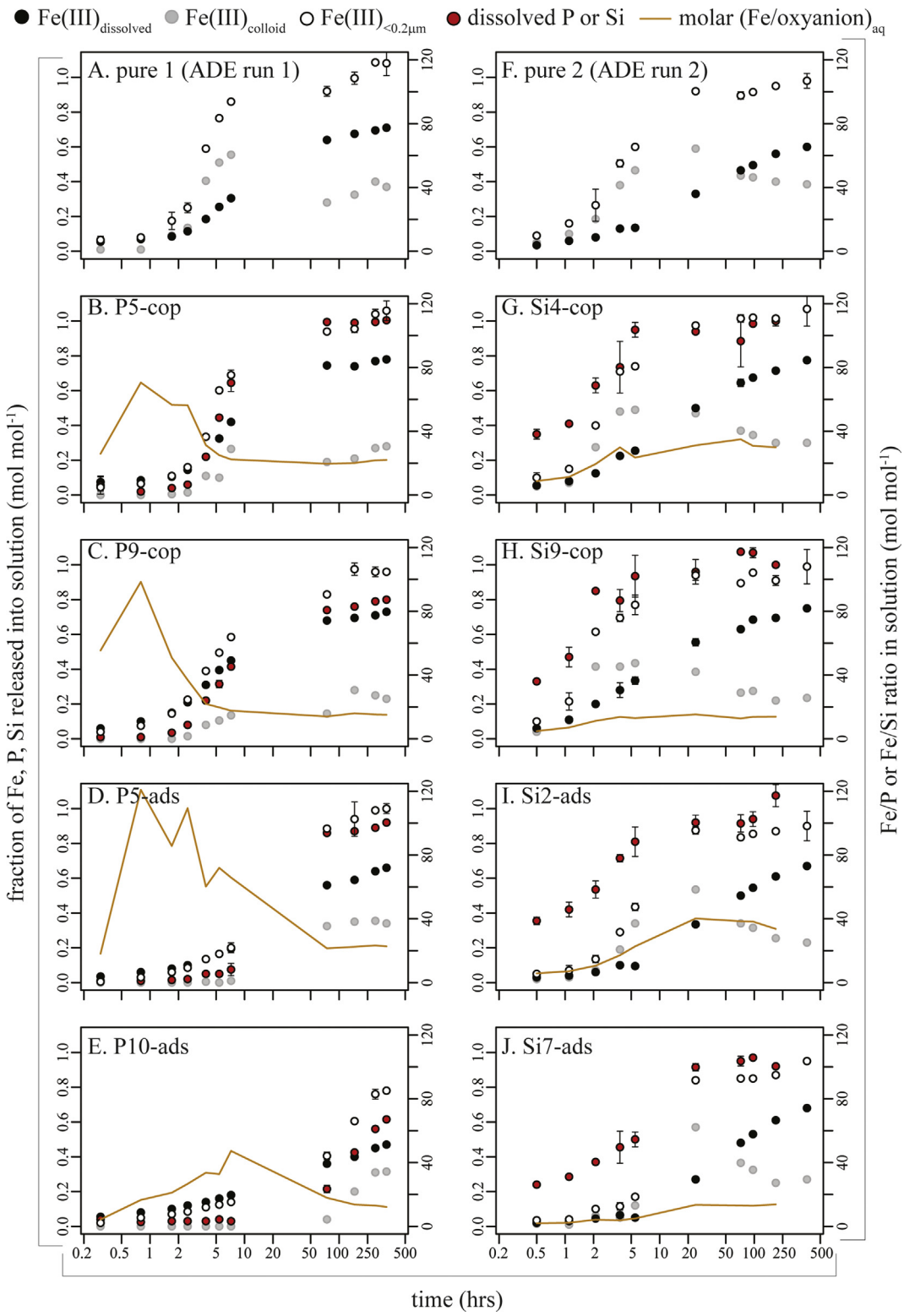

Fig. 3. Kinetics of total Fe < 0.2 µm (white), dissolved Fe (black), colloidal Fe (gray) and soluble reactive P and Si (red) accumulation in the acidic dissolution experiment (0.01 mol L^{-1} HCl, pH 2) for the different types of FeOx. Orange lines show solution $Fe_{dissolved}$/(P or Si) ratio. Pure FeOx 1 was part of ADE series 1, which included 2L-Fh and all P-bearing Fe(III) phases in duplicate. Pure FeOx 2 was part of ADE series 2 with all Si-bearing FeOx. All symbols represent the mean and error bars represent the standard deviation ($n = 2$). Note the logarithmic x axis. (For interpretation of the references to color in this figure legend, the reader is referred to the Web version of this article.)

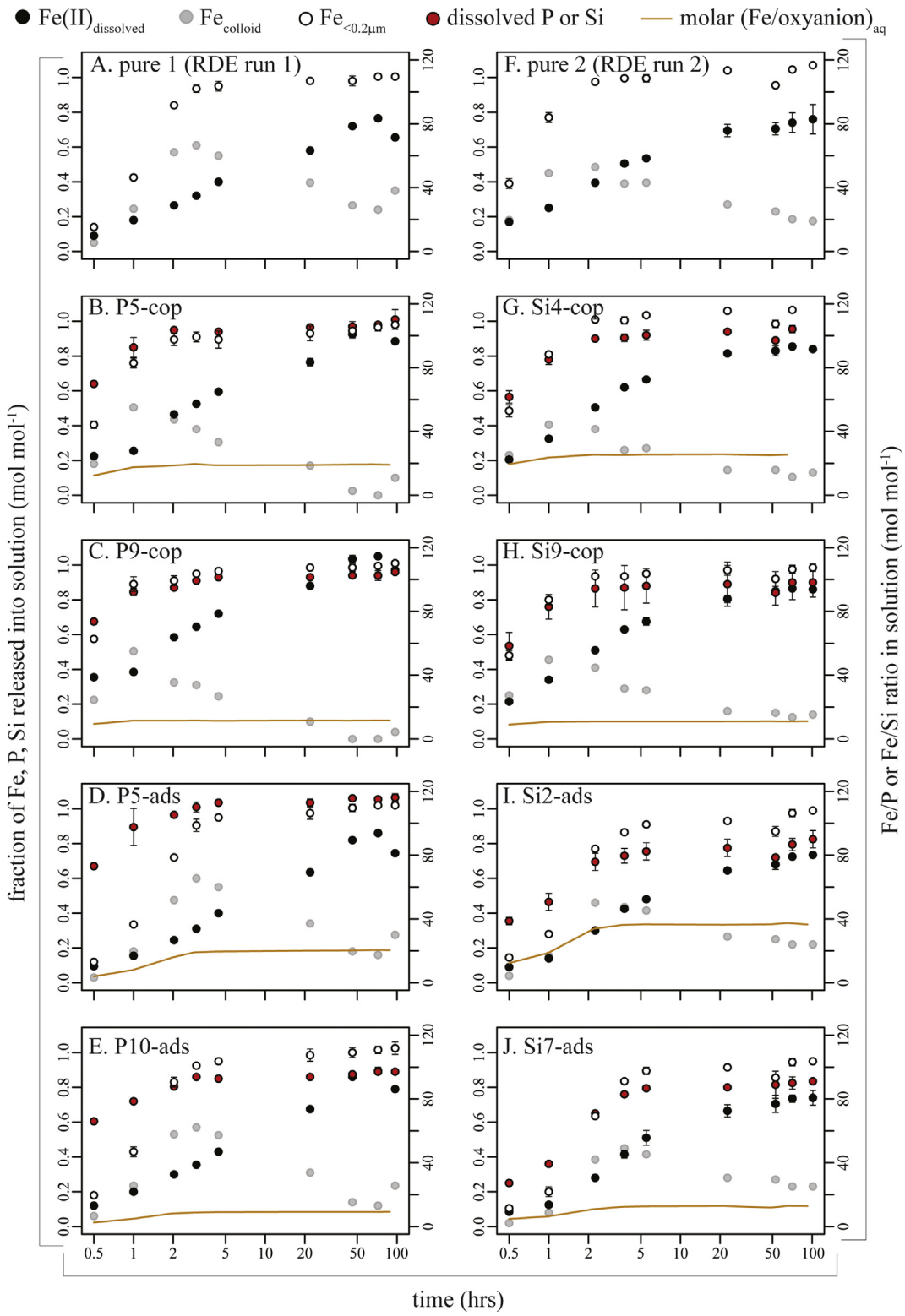

Fig. 4. Kinetics of total Fe < 0.2 µm (white), dissolved Fe (black), colloidal Fe (gray) and soluble reactive P and Si (red) accumulation in the reductive dissolution experiment (20 g L^{-1} ascorbic acid, pH 7.8) for the different types of FeOx. Orange lines show solution $Fe_{dissolved}$/(P or Si) ratio. Pure FeOx 1 was part of RDE series 1, which included 2L-Fh and all P-bearing Fe(III) phases in duplicate. Pure FeOx 2 was part of RDE series 2 with all Si-bearing FeOx. All symbols represent the mean and error bars represent the standard deviation ($n = 2$). Note the logarithmic x axis. (For interpretation of the references to color in this figure legend, the reader is referred to the Web version of this article.)

2
Fitting parameters for FeOx dissolution kinetics under acidic (0.01 mol L^{-1} HCl, pH 3) or circumneutral reducing (20 g L^{-1} ascorbic acid, pH 7.8) conditions. See section 2.6 for details on the meaning of k' and γ. For all experiments, the fit of the dissolution rate equation had $R^2 > 0.95$.

	ADE		RDE	
	k'	γ	k'	γ
pure FeOx	2.3e-05	4.4	7.5e-05	4.1
P5-cop FeOx	3.2e-05	3.7	1.3e-04	2.6
P9-cop FeOx	5.8e-05	4.9	2.3e-04	2.4
P5-ads FeOx	1.5e-05	4.7	4.9e-05	2.7
P10-ads FeOx	2.3e-05	9.8	6.3e-05	2.7
Si4-cop FeOx	2.6e-05	3.9	1.7e-04	3.2
Si9-cop FeOx	4.8e-05	4	1.7e-04	3.1
Si2-ads FeOx	8.2e-06	2.8	7.0e-05	3.8
Si7-ads FeOx	5.5e-06	2.5	5.0e-05	3.4

The P/Fe and Si/Fe ratios used in this study were relevant for natural systems (up to 0.1) and generally lower than those applied in the aforementioned studies. Consequently, we observed more subtle effects of P and Si coprecipitation on FeOx structure. Specifically, our results show a decrease in the magnitude peak arising from corner-sharing Fe–Fe bonds in both the Fe EXAFS (~3.1 Å) and HEXS (~3.4 Å) data (Fig. 1D – F, Fig. 2). Additionally, the HEXS results showed increased magnitude peaks for P-cop FeOx and Si-cop FeOx compared to 2L-Fh at ~1.6 Å and ~3.2 Å, arising from Si/P–O and Si/P–Fe bonds, respectively (van Genuchten et al., 2014). The HEXS data also showed that the impact of P or Si coprecipitation increased with oxyanion loading, and that at similar loading the impact of P coprecipitation exceeded that of Si coprecipitation (as evident at the three highlighted interatomic distances 1.6, 3.2 and 3.4 Å in the PDFs in Fig. 3). In addition, at the highest P loading (Fe/P = 0.1) the particle size as reflected in the coherent scattering domain of the PDF decreased from ~0.2 to 0.15 nm (Fig. 2A).

Overall, the EXAFS and HEXS results show that the presence of P and Si during FeOx formation by base hydrolysis of a concentrated Fe(III) solution has a minor impact on the structure of the already poorly ordered FeOx that forms under such experimental conditions. Based on structural alteration as probes by EXAFS and HEXS, we would therefore expect a minor impact of P and Si coprecipitation, notwithstanding the impact that interaction with oxyanions can have on the macroscopic properties of FeOx such as aggregation (e.g. Cornell et al., 1987; Paige et al., 1997b; van Genuchten et al., 2014).

4.2. FeOx dissolution kinetics and the impact of interaction with P, Si

4.2.1. Aging effects on FeOx reactivity

The minor differences in the Fe EXAFS and HEXS spectra of fresh and aged 2L-Fh (Figs. 1 and 2) suggest that structural alteration of the 2L-Fh during four weeks of aging was insignificant. Nonetheless, we observed differences in 2L-Fh dissolution between repeated runs that were two weeks apart for both ADE and RDE (Fig. 3A, F, 4A, F). Variations in pure FeOx dissolution rates do not correlate with the age of the suspensions: dissolution of pure FeOx was slower during run 2 of the ADE, while it was faster during run 2 of the RDE. The small standard deviations for duplicates of each specific FeOx within an experimental run argue against major

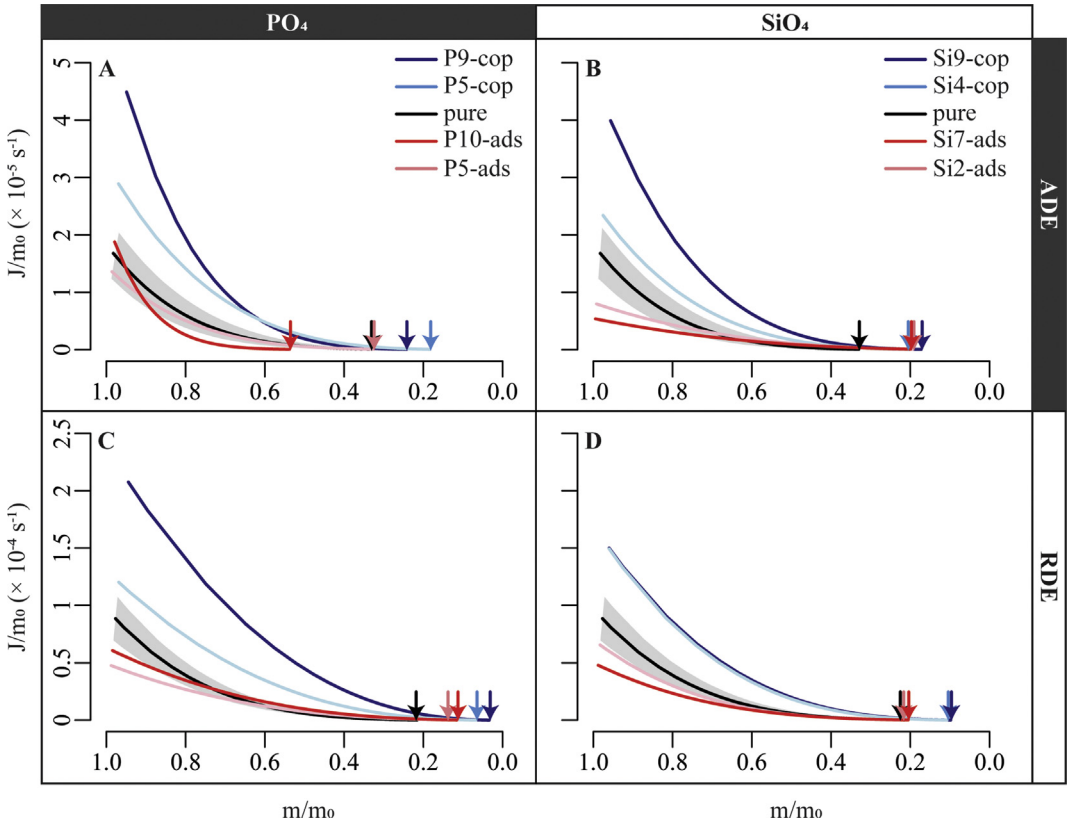

Fig. 5. Normalized dissolution rate (J/m_0 in s^{-1}) plotted against fraction of remaining FeOx (m/m_0) for the investigated synthetic FeOx. Top panels show results for P-bearing FeOx (A) and Si-bearing FeOx (B) during acidic dissolution (ADE), bottom panels show results for P-bearing FeOx (C) and Si-bearing FeOx (D) during reductive dissolution. For 2L-Fh, the dissolution rate curves for the two runs per experiment (ADE or RDE; 4 runs in total, all in duplicate) are shown as dashed lines, the mean of the two runs is shown as black line. Vertical arrows indicate the fraction of each FeOx that remained at the end of each experiment.

random variation in dissolution behavior. Furthermore, the different FeOx used in this study (no, coprecipitated or adsorbed phosphate and silicate) were likely differently affected by mineral aging (Cornell et al., 1987; Senn et al., 2017). Considering these uncertainties, we use the average pure FeOx dissolution rate to assess the impact of adsorption or coprecipitation of P and Si on FeOx dissolution kinetics.

4.2.2. Kinetics of acidic versus reductive dissolution

The dissolution rate was about an order of magnitude higher in the RDE compared to ADE (Fig. 5). This can be attributed to the formation of easily detachable complexes of reduced Fe(II) and ligands at the particle surface during RDE (Zinder et al., 1986) that results in more rapid mineral dissolution than occurs due to proton-induced bond weakening during ADE. All components of the citrate-bicarbonate-ascorbic acid solution used for RDE can adsorb onto the surface of FeOx particles and thus contribute to surface complex detachment (Kallay and Matijevic, 1985; van Geen et al., 1994; Deng, 1997; Nemade et al., 2007). The concentration of ligands was sufficient to saturate all FeOx surface sites, which also explains the rapid release of P and Si into solution during the RDE, and the apparent lack of readsorption (Figs. 3 and 4).

4.2.3. Contrasting effects of oxyanion coprecipitation and adsorption on FeOx reactivity

Coprecipitation of P and Si at the low initial oxyanion/Fe ratios in this study (0.04–0.1) had a relatively minor impact on mineral structure, with subtle decreases in structural coherency compared to 2L-Fh as probed by EXAFS and HEXS (Figs. 1 and 2). Yet, the dissolution rates of P-cop FeOx and Si-cop FeOx during the ADE and RDE increased relative to that of pure FeOx (Fig. 5). The dissolution rate increased with P or Si loading, with highest rates observed for P9-cop FeOx, which consisted of smaller crystallites (~1.5 nm) compared to all other FeOx (~2 nm). Considering that P and Si coprecipitation at the chosen loadings resulted in only minor structural FeOx alteration, our results indicate that FeOx formation in the presence of P or Si affected the macroscopic properties of FeOx and thereby FeOx dissolution. For instance, occupation of FeO_6 surface sites by phosphate or silicate during Fe(III) particle formation can inhibit particle aggregation (Kaegi et al., 2010). This would not be detected by the employed X-ray techniques that are sensitive to short-range structure, but can impact overall reactivity.

While oxyanion coprecipitation increased FeOx reactivity, adsorption of P and Si resulted in decreased FeOx dissolution rates. This is in line with earlier work that showed adsorption of oxyanions such as phosphate and AsO_4 stabilized FeOx mineral surfaces and decreased FeOx reactivity (Biber et al., 1994; Jones et al., 2009; Majzlan, 2011). Assuming that a molar P/Fe ratio (Γ_{PO4}) of ~0.2 corresponds to saturation of reactive surface sites for pure 2L-Fh (Dzombak and Morel, 1990), only up to about half of the available reactive surface sites became occupied during our experiments. In addition, Si was adsorbed onto FeOx at lower loadings (oxyanion/Fe ratios) than P but Si-ads FeOx showed lower dissolution rates than P-ads FeOx (Fig. 5), further suggesting that occupation of surface sites is not the only factor determining the dissolution behavior of FeOx with adsorbed P or Si. We therefore propose that the decreased reactivity of FeOx with adsorbed P or Si at low loadings may be the result of occupation of reactive surface sites as well as particle aggregation, promoted by sorption of P and Si onto pre-existing FeOx surfaces (Cornell et al., 1987; Paige et al., 1997b). As such, altered macroscopic mineral properties may contribute to the opposite effects of coprecipitation and adsorption on FeOx reactivity.

All dissolution experiments showed a transient increase in $Fe_{colloid}$ (= $Fe_{<0.2\mu m}$ - $Fe_{dissolved}$), suggesting the presence of nanoparticles < 0.2 μm in the first 1–10 h of the experiments. The onset of colloid release occurs after dissolution of 15–20% of FeOx in all experiments, which could signify a common change in dissolution mechanism from surface dissolution to detachment of nanoparticles from the original FeOx solid phase. During acidic dissolution, oxyanion coprecipitation as well as adsorption limits the release of colloidal Fe into solution, in particular for P-bearing FeOx (Fig. 3A – E). However, the normalized dissolution rate of P-cop FeOx exceeds that of P-ads FeOx (Fig. 5A). This suggests that colloidal Fe released from P-cop FeOx is relatively unstable and dissolves rapidly, while release of colloidal Fe from P-ads FeOx is limited; overall the dissolution of P-ads FeOx proceeds more slowly.

4.2.4. Timing and stoichiometry of oxyanion release during FeOx dissolution

Besides differences in FeOx dissolution behavior as assessed from dissolved Fe data, we observed differences in the release of Fe and P or Si during FeOx dissolution. During RDE, P and Si were both rapidly released from the FeOx surface from all FeOx (Fig. 4), likely because of the aforementioned competition of added ligands with P and Si for surface sites (section 4.2.2). By contrast, the temporal release patterns during the ADE differed markedly for P and Si. Release of Si was rapid for Si-ads FeOx as well as Si-cop FeOx and initially exceeded Fe accumulation in solution: 25–35% of total Si was in solution at the first sampling point, compared to <10% of $Fe(III)_{<0.2\mu m}$ (Fig. 3G – J). This suggests that Si release was initially related to desorption rather than FeOx dissolution. The Si binding capacity of FeOx decreases at pH < 9 because Si adsorption results in a net release of H^+ (Davis et al., 2002; Hiemstra et al., 2007). After the initial phase characterized by Si desorption, release of Si was more rapid for Si-cop FeOx than Si-ads Fh (Fig. 3), in line with the difference in FeOx dissolution rates (Fig. 5).

Trends in the stoichiometry of Fe and P release during acidic dissolution of P-bearing FeOx were very different to those observed during acidic dissolution of Si-bearing FeOx. For both P-cop FeOx and P-ads FeOx, P release was limited during the initial stages of FeOx dissolution, resulting in high $Fe(III)_{dissolved}$/P ratios (Fig. 3). We attribute the initial incongruent dissolution to readsorption of P onto remaining FeOx surface sites at pH 2 of the ADE, as the P sorption capacity of FeOx remains high at this pH (Antelo et al., 2005, 2010). This readsorption may act to stabilize the surface of P-cop during dissolution and thus modulate its dissolution rate, but such an effect cannot be extracted from the available data.

The release of P into solution commenced when 15–20% of FeOx was dissolved. The calculated solid-phase P/Fe ratios (0.06–0.12) at this point were still below the maximum P loading of 2L-Fh of ~0.2 as was found previously (Dzombak and Morel, 1990) and confirmed by our P sorption data (P/Fe ≈ 0.22 at pH 6). Therefore, depletion of accessible binding sites seems an unlikely explanation for the onset of P accumulation in solution. The timing of P release from the solid phase coincides with an observed increase in the $Fe_{colloid}$ fraction. The aforementioned change in FeOx dissolution behavior from surface dissolution to release of Fe nanoparticles into solution may then have also affected P release. Soluble reactive P (SRP) as measured by the molybdenum-blue method is determined in an acidic (pH < 1) medium containing dilute sulfuric acid that could rapidly dissolve P-bearing Fe colloids. As a result, the pool of soluble reactive P measured by this method could include dissolved P as well as P associated with these colloids.

5. Conclusions and implications

Interactions between FeOx and phosphate or silicate affect the structure and stability of the resulting oxyanion-bearing FeOx. The nature of the resulting effects depends strongly on whether the

interaction occurs during or subsequent to FeOx formation. Coprecipitation of phosphate or silicate during FeOx formation decreases the degree of structural order and may inhibit particle aggregation, thereby enhancing FeOx dissolution rates under acidic and reducing conditions. Conversely, adsorption stabilizes the mineral surface and may enhance particle aggregation, leading to decreased dissolution rates. These effects are apparent even during coprecipitation with oxyanion/Fe ratios as low as 0.04 mol mol^{-1}. At these low P and Si loadings, Fe K-edge EXAFS and HEXS data show only minor changes to the structural properties of the FeOx, suggesting that alteration of macroscopic mineral properties (i.e. aggregation) plays a prominent role. The dissolution behavior of FeOx and the fate of associated oxyanions vary on timescales (days, weeks) that are relevant for dynamic natural systems. As such, increased pore water concentrations of oxyanions such as phosphate and silicate – as caused, for instance, by eutrophication – may enhance oxyanion coprecipitation, decrease mineral stability and eventually suppress the nutrient retention capacity of sediments with strong temporal and vertical redox gradients. This feedback in the eutrophication process of aquatic systems, which is so far unrecognized, should be further explored in light of the human-induced increase of nutrient delivery to aquatic systems and expansion of coastal areas with oxygen-depleted bottom waters.

Acknowledgements

This work was funded by a grant from the Netherlands Organisation for Scientific Research, NWO Veni grant 863.14.014 to P. Kraal. Case M. van Genuchten acknowledges NWO Veni grant 14400. The work was further supported by a NWO DUBBLE grant 195.068.1039 for ESRF beamline BM26A. We gratefully thank the technical support and advice of Dipanjan Banerjee at the DUBBLE beamline during Fe K-edge EXAFS data collection. Simon Müller kindly assisted with data collection at ESRF. We thank the reviewer for valuable feedback.

Appendix A. Supplementary data

Supplementary data to this article can be found online at https://doi.org/10.1016/j.chemosphere.2019.06.071.

References

Antelo, J., Avena, M., Fiol, S., López, R., Arce, F., 2005. Effects of pH and ionic strength on the adsorption of phosphate and arsenate at the goethite–water interface. J. Colloid Interface Sci. 285 (2), 476–486.
Antelo, J., Fiol, S., Pérez, C., Mariño, S., Arce, F., Gondar, D., López, R., 2010. Analysis of phosphate adsorption onto ferrihydrite using the CD-MUSIC model. J. Colloid Interface Sci. 347 (1), 112–119.
APHA, 2005. Standard Methods for the Examination of Water and Wastewater. American Public Health Association - American Water Works Association - Water Environment Federation.
Biber, M.V., dos Santos Afonso, M., Stumm, W., 1994. The coordination chemistry of weathering: IV. Inhibition of the dissolution of oxide minerals. Geochem. Cosmochim. Acta 58 (9), 1999–2010.
Boland, D.D., Collins, R.N., Miller, C.J., Glover, C.J., Waite, T.D., 2014. Effect of solution and solid-phase conditions on the Fe(II)-accelerated transformation of ferrihydrite to lepidocrocite and goethite. Environ. Sci. Technol. 48 (10), 5477–5485.
Borch, T., Masue, Y., Kukkadapu, R.K., Fendorf, S., 2007. Phosphate imposed limitations on biological reduction and alteration of ferrihydrite. Environ. Sci. Technol. 41 (1), 166–172.
Borsboom, M., Bras, W., Cerjak, I., Detollenaere, D., van Loon, D.G., Goedtkind, P., Konijnenburg, M., Lassing, P., Levine, Y.K., Munneke, B., Oversluizen, M., van Tol, R., Vlieg, E., 1998. The Dutch-Belgian beamline at the ESRF. J. Synchrotron Radiat. 5, 518–520.
Buffle, J., De Vitre, R.R., Perret, D., Leppard, G.G., 1989. Physico-chemical characteristics of a colloidal iron phosphate species formed at the oxic-anoxic interface of a eutrophic lake. Geochem. Cosmochim. Acta 53 (2), 399–408.
Chapman, K.W., Chupas, P.J., 2013. Pair distribution function analysis of high-energy X-ray scattering data. In: Rodriguez, J.A., Hanson, J.C., Chupas, P.J. (Eds.), In-situ Characterization of Heterogeneous Catalysts. John Wiley and Sons, Inc.
Chupas, P.J., Qiu, X., Hanson, J.C., Lee, P.L., Grey, C.P., Billinge, S.J.L., 2003. Rapid-acquisition pair distribution function (RA-PDF) analysis. J. Appl. Crystallogr. 36 (6), 1342–1347.
R.CoreTeam, 2013. R: A Language and Environment for Statistical Computing (Vienna, Austria).
Cornell, R.M., Giovanoli, R., Schindler, P.W., 1987. Effect of silicate species on the transformation of ferrihydrite into goethite and hematite in alkaline media. Clay Clay Miner. 35 (1), 21–28.
Davis, C.C., Chen, H.-W., Edwards, M., 2002. Modeling silica sorption to iron hydroxide. Environ. Sci. Technol. 36 (4), 582–587.
Deng, Y., 1997. Effect of pH on the reductive dissolution rates of iron(III) hydroxide by ascorbate. Langmuir 13 (6), 1835–1839.
Dzombak, D.A., Morel, F.M.M., 1990. Surface Complexation Modeling: Hydrous Ferric Oxide. Wiley, New York, p. 416.
Farrow, C.L., Juhas, P., Liu, J.W., Bryndin, D., Božin, E.S., Bloch, J., Proffen, T., Billinge, S.J.L., 2007. PDFfit2 and PDFgui: computer programs for studying nanostructure in crystals. J. Phys. Condens. Matter. 19 (33), 335219.
Hammersley, A.P., Svensson, S.O., Hanfland, M., Fitch, A.N., Hausermann, D., 1996. Two-dimensional detector software: from real detector to idealised image or two-theta scan. High Press. Res. 14 (4–6), 235–248.
Hiemstra, T., 2013. Surface and mineral structure of ferrihydrite. Geochem. Cosmochim. Acta 105 (0), 316–325.
Hiemstra, T., Barnett, M.O., van Riemsdijk, W.H., 2007. Interaction of silicic acid with goethite. J. Colloid Interface Sci. 310 (1), 8–17.
Hyacinthe, C., Bonneville, S., Van Cappellen, P., 2006. Reactive iron(III) in sediments: chemical versus microbial extractions. Geochem. Cosmochim. Acta 70 (16), 4166–4180.
Jambor, J.L., Dutrizac, J.E., 1998. Occurrence and constitution of natural and synthetic ferrihydrite, a widespread iron oxyhydroxide. Chem. Rev. 98 (7), 2549–2586.
Jones, A.M., Collins, R.N., Rose, J., Waite, T.D., 2009. The effect of silica and natural organic matter on the Fe(II)-catalysed transformation and reactivity of Fe(III) minerals. Geochem. Cosmochim. Acta 73 (15), 4409–4422.
Kaegi, R., Voegelin, A., Folini, D., Hug, S.J., 2010. Effect of phosphate, silicate, and Ca on the morphology, structure and elemental composition of Fe(III)-precipitates formed in aerated Fe(II) and As(III) containing water. Geochem. Cosmochim. Acta 74 (20), 5798–5816.
Kallay, N., Matijevic, E., 1985. Adsorption at solid/solution interfaces. 1. Interpretation of surface complexation of oxalic and citric acids with hematite. Langmuir 1 (2), 195–201.
Kelly, S.D., Hesterberg, D., Ravel, B., 2008. Analysis of soils and minerals using X-ray absorption spectroscopy. In: Ulery, A.L., Drees, L.R. (Eds.), Methods of Soil Analysis Part 5—Mineralogical Methods. Soil Science Society of America, Madison, Wisconsin.
Kraal, P., Dijkstra, N., Behrends, T., Slomp, C.P., 2017. Phosphorus burial in sediments of the sulfidic deep Black Sea: key roles for adsorption by calcium carbonate and apatite authigenesis. Geochem. Cosmochim. Acta 204, 140–158.
Kukkadapu, R.K., Zachara, J.M., Fredrickson, J.K., Kennedy, D.W., 2004. Biotransformation of two-line silica-ferrihydrite by a dissimilatory Fe(III)-reducing bacterium: formation of carbonate green rust in the presence of phosphate1. Geochem. Cosmochim. Acta 68 (13), 2799–2814.
Larsen, O., Postma, D., 2001. Kinetics of reductive bulk dissolution of lepidocrocite, ferrihydrite, and goethite. Geochem. Cosmochim. Acta 65 (9), 1367–1379.
Majzlan, J., 2011. Thermodynamic stabilization of hydrous ferric oxide by adsorption of phosphate and arsenate. Environ. Sci. Technol. 45 (11), 4726–4732.
Michel, F.M., Ehm, L., Antao, S.M., Lee, P.L., Chupas, P.J., Liu, G., Strongin, D.R., Schoonen, M.A.A., Phillips, B.L., Parise, J.B., 2007. The structure of ferrihydrite, a nanocrystalline material. Science 316 (5832), 1726–1729.
Mullin, J.B., Riley, J.P., 1955. The colorimetric determination of silicate with special reference to sea and natural waters. Anal. Chim. Acta 12, 162–176.
Nemade, P., Kadam, A.M., Oza, G., Dutta, S.M., Shankar, U.S., 2007. Effects of anions on arsenic adsorption with iron hydroxide - a review. Indian J. Environ. Prot. 27 (12), 1057–1064.
Nikitenko, S., Beale, A.M., van der Eerden, A.M.J., Jacques, S.D.M., Leynaud, O., O'Brien, M.G., Detollenaere, D., Kaptein, R., Weckhuysen, B.M., Bras, W., 2008. Implementation of a combined SAXS/WAXS/QEXAFS set-up for time-resolved in situ experiments. J. Synchrotron Radiat. 15 (6), 632–640.
Norkko, J., Reed, D.C., Timmermann, K., Norkko, A., Gustafsson, B.G., Bonsdorff, E., Slomp, C.P., Carstensen, J., Conley, D.J., 2012. A welcome can of worms? Hypoxia mitigation by an invasive species. Glob. Chang. Biol. 18 (2), 422–434.
Paige, C.R., Snodgrass, W.J., Nicholson, R.V., Scharer, J.M., 1997a. An arsenate effect on ferrihydrite dissolution kinetics under acidic oxic conditions. Water Res. 31 (9), 2370–2382.
Paige, C.R., Snodgrass, W.J., Nicholson, R.V., Scharer, J.M., He, Q.H., 1997b. The effect of phosphate on the transformation of ferrihydrite into crystalline products in alkaline media. Water, Air, Soil Pollut. 97 (3), 397–412.
Pham, A.N., Rose, A.L., Feitz, A.J., Waite, T.D., 2006. Kinetics of Fe(III) precipitation in aqueous solutions at pH 6.0–9.5 and 25°C. Geochem. Cosmochim. Acta 70 (3), 640–650.
Pokrovski, G.S., Schott, J., Farges, F., Hazemann, J.-L., 2003. Iron (III)-silica interactions in aqueous solution: insights from X-ray absorption fine structure spectroscopy. Geochem. Cosmochim. Acta 67 (19), 3559–3573.
Postma, D., 1993. The reactivity of iron oxides in sediments: a kinetic approach. Geochem. Cosmochim. Acta 57 (21–22), 5027–5034.

Ravel, B., Newville, M., 2005. Athena, Artemis, Hephaestus: data analysis for X-ray absorption spectroscopy using IFEFFIT. J. Synchrotron Radiat. 12, 537–541.
Rose, S., Ghazi, A.M., 1998. Experimental study of the stability of metals associated with iron oxyhydroxides precipitated in acid mine drainage. Environ. Geol. 36 (3), 364–370.
Rose, J., Manceau, A., Bottero, J.-Y., Masion, A., Garcia, F., 1996. Nucleation and growth mechanisms of Fe oxyhydroxide in the presence of PO4 ions. 1. Fe K-edge EXAFS study. Langmuir 12 (26), 6701–6707.
Schoepfer, V.A., Burton, E.D., Johnston, S.G., Kraal, P., 2017. Phosphate-imposed constraints on schwertmannite stability under reducing conditions. Environ. Sci. Technol. 51 (17), 9739–9746.
Schwertmann, U., Cornell, S., 1991. Iron Oxides in the Laboratory: Preparation and Characterization. Wiley, p. 188.
Senn, A.-C., Kaegi, R., Hug, S.J., Hering, J.G., Mangold, S., Voegelin, A., 2015. Composition and structure of Fe(III)-precipitates formed by Fe(II) oxidation in water at near-neutral pH: interdependent effects of phosphate, silicate and Ca. Geochem. Cosmochim. Acta 162 (0), 220–246.
Senn, A.-C., Kaegi, R., Hug, S.J., Hering, J.G., Mangold, S., Voegelin, A., 2017. Effect of aging on the structure and phosphate retention of Fe(III)-precipitates formed by Fe(II) oxidation in water. Geochem. Cosmochim. Acta 202, 341–360.
Strickland, J.D., Parsons, T.R., 1972. A practical handbook of seawater analysis, Bulletin, vol. 167. Fish. Res. Board Canada.
Stumm, W., 1997. Reactivity at the mineral-water interface: dissolution and inhibition. Colloid. Surf. Physicochem. Eng. Asp. 120 (1), 143–166.
van Geen, A., Robertson, A.P., Leckie, J.O., 1994. Complexation of carbonate species at the goethite surface: implications for adsorption of metal ions in natural waters. Geochem. Cosmochim. Acta 58 (9), 2073–2086.
van Genuchten, C.M., Peña, J., 2016. Antimonate and arsenate speciation on reactive soil minerals studied by differential pair distribution function analysis. Chem. Geol. 429, 1–9.
van Genuchten, C.M., Peña, J., Amrose, S.E., Gadgil, A.J., 2014. Structure of Fe(III) precipitates generated by the electrolytic dissolution of Fe(0) in the presence of groundwater ions. Geochem. Cosmochim. Acta 127, 285–304.
Voegelin, A., Kaegi, R., Frommer, J., Vantelon, D., Hug, S.J., 2010. Effect of phosphate, silicate, and Ca on Fe(III)-precipitates formed in aerated Fe(II)- and As(III)-containing water studied by X-ray absorption spectroscopy. Geochem. Cosmochim. Acta 74 (1), 164–186.
Voegelin, A., Senn, A.-C., Kaegi, R., Hug, S.J., Mangold, S., 2013. Dynamic Fe-precipitate formation induced by Fe(II) oxidation in aerated phosphate-containing water. Geochem. Cosmochim. Acta 117 (0), 216–231.
Waychunas, G.A., Rea, B.A., Fuller, C.C., Davis, J.A., 1993. Surface chemistry of ferrihydrite: Part 1. EXAFS studies of the geometry of coprecipitated and adsorbed arsenate. Geochem. Cosmochim. Acta 57 (10), 2251–2269.
Webster, J.G., Swedlund, P.J., Webster, K.S., 1998. Trace metal adsorption onto an acid mine drainage iron(III) oxy hydroxy sulfate. Environ. Sci. Technol. 32 (10), 1361–1368.
Zinder, B., Furrer, G., Stumm, W., 1986. The coordination chemistry of weathering: II. Dissolution of Fe(III) oxides. Geochem. Cosmochim. Acta 50 (9), 1861–1869.